LWT - Food Science and Technology 246 (2026) 119277

Contents lists available at ScienceDirect

LWT

journal homepage: www.elsevier.com/locate/lwt

3D printing food ink development using *Auxenochlorella protothecoides*: Rheology, printability, and fish texture simulations

Yurim Ha [a,1], Eui-Jung Han [a,1], Yourim Oh [a,b,*], Jin-Kyu Rhee [a,b,**]

[a] Department of Food Science and Biotechnology, Ewha Womans University, Seoul, 03760, Republic of Korea
[b] SuFAB Inc., 123 Digital-ro 26-gil, Guro District, Seoul, South Korea

ARTICLE INFO

Keywords:
White *Auxenochlorella protothecoides*
Rheological properties
3D-printing parameter
Texture properties
Fish texture

ABSTRACT

This study explores the potential of microalga (*Auxenochlorella protothecoides*) as seafood ink for a three-dimensional (3D)-printed product that replicates fish texture. Food inks were prepared with varying concentrations of microalga and their suitability for 3D-printing was evaluated through a rheological analysis. The concentration showing the highest printability was then selected to assess the effects of 3D-printing parameters on the texture of printed samples. Initially, the food ink was suitable for 3D printing across all microalga concentrations due to its shear-thinning behavior, but increasing microalga content lowered the flow index and reduced printability. Optimal printability was achieved at a microalga concentration of 36%, where both height and width percentage errors were 0%, closely matching the computer-aided design. Using this ink, the physical properties of the 3D-printed models were examined based on printing parameters. Various physical properties depended on the nozzle diameter and infill density, with the resulting textures closely matching those salmon, mackerel, and flounder. These findings suggest that microalga can be used as food ink in 3D printing of fish substitutes that replicate the texture of real fish.

1. Introduction

Global seafood consumption has been increasing at nearly twice the rate of population growth (FAO, 2024). This increase has been associated with significant ecological consequences, including overfishing, loss of marine biodiversity, and heightened concerns about consumer exposure to marine pollutants, such as mercury and microplastics, both of which pose critical environmental and public health concerns (Teixeira & Silva, 2024). In response, the seafood industry has accelerated the development of alternative products — commonly referred to as fish analogs — that replicate the appearance, taste, and texture of conventional fish while aiming to reduce ecological and health risks (Li et al., 2024).

Microalgae are considered a sustainable source of high protein food products. For example, several commercial chlorella and *Auxenochlorella* biomasses are composed of approximately 65% protein on a dry-matter basis, although biomass composition can vary with cultivation conditions (Canelli et al., 2020; Coleman et al., 2022). Among these algae, *Auxenochlorella protothecoides*, a white-pigmented strain of chlorella (WC) offers several advantages. Its pale pigmentation, achieved through heterotrophic cultivation and pigment biosynthesis regulation (Clydesdale, 1993), provides superior visual compatibility for analogs of white-fleshed seafood, an objective that is challenging to achieve with green-pigmented algae. Additionally, its classification as "generally recognized as safe" reinforces its food-grade ingredient applicability (Torres-Tiji et al., 2020). Prior research has used microalgae as food additives and coloring agents, (Batista et al., 2017; García-Segovia et al., 2017), but their suitability as a primary fish analog remains unexplored.

Meanwhile, three-dimensional (3D) printing has created new possibilities in customized food fabrication, enabling precise control of product shape, internal structure, and texture (Mantihal et al., 2020). A critical factor in the 3D printing of food products is the development of inks with rheological and mechanical properties that ensure stable extrusion and shape retention (Chen et al., 2022). These performance outcomes can be influenced by both formulation variables (e.g., biomass concentration) and printing parameters (e.g., nozzle diameter and infill density) (Oh et al., 2024). Such parameters can affect printability,

* Corresponding author. Department of Food Science and Biotechnology, Ewha Womans University, Seoul, 03760, Republic of Korea.
** Corresponding author. Department of Food Science and Biotechnology, Ewha Womans University, Seoul, 03760, Republic of Korea.
E-mail addresses: gler114@ewhain.net (Y. Oh), jkrhee@ewha.ac.kr (J.-K. Rhee).
[1] Both authors contributed equally.

https://doi.org/10.1016/j.lwt.2026.119277
Received 6 June 2025; Received in revised form 12 March 2026; Accepted 14 March 2026
Available online 14 March 2026
0023-6438/© 2026 The Authors. Published by Elsevier Ltd. This is an open access article under the CC BY license (http://creativecommons.org/licenses/by/4.0/).

dimensional fidelity, and textural properties of 3D-printed foods (Huang et al., 2019; Liu et al., 2018). Understanding and optimizing these parameters is therefore essential for the fabrication of high-quality 3D-printed foods.

Despite growing interest in 3D-printed fish analogs, most reported formulations rely on plant-derived proteins combined with hydrocolloids to reproduce a seafood-like texture and appearance (Shi et al., 2023; Zhong et al., 2023). However, microalga-based systems, particularly those involving *A. protothecoides,* have rarely been investigated as a single-ingredient printable matrix (Mirzapour-Kouhdasht et al., 2024). The printability and rheological-textural attributes of *A. protothecoides* biomass as a stand-alone ink for 3D printing remain to be systematically evaluated.

This study aims to develop and characterize *A. protothecoides* food ink to emulate the fish-like texture. We first evaluated its rheological behavior and related it to extrusion stability and dimensional fidelity to identify the optimal concentration. Using the selected concentration, we examined how nozzle diameter and infill density influence the textural properties of 3D-printed constructs by comparing the resulting texture profiles with those of three fish species (mackerel, flounder, and salmon).

2. Materials and methods

2.1. Material

White chlorella (*A. protothecoides*) dry powder (hereafter referred to as WC) was obtained from Daesang Corp.(Seoul, Korea). Fresh samples of salmon, mackerel, and flounder were purchased from a local market in Seoul, Korea.

2.2. Preparation of food ink

Food inks derived from WC were prepared by homogenizing dry biomass in distilled water for 5 min at room temperature, using varying proportions (32%, 34%, 36%, 38%, and 40%) (w/w), of WC as 32% (w/w) was identified as the minimum gelation concentration in preliminary experiments. After preparation, all inks were kept at 4 °C overnight for adequate rehydration and labeled as follows: WC 32%, WC 34%, WC 36%, WC 38%, and WC 40%.

2.3. Microstructure

The microstructure of WC inks was analyzed using a TM3030Plus tabletop scanning electron microscope (SEM) (Hitachi High-Technologies, Japan). Sample preparation was performed with slight modifications to a previously reported method (Oh et al., 2024). Briefly, WC inks were cast into silicone molds and frozen in a deep freezer for 18 h. The samples were then freeze-dried for 48 h. Each sample was attached to an SEM stub using double-sided carbon tape. The samples were visualized under the microscope at an accelerating voltage of 15 kV and captured at a magnification of 600 × .

2.4. Measurement of rheological properties

For rheological characterization of the used food inks, rheological measurements were performed according to a procedure described by (Maldonado-Rosas et al., 2022). The rheological properties of the samples were measured at 25 °C with an MCR102 rheometer (Anton Paar, Austria) using 25 mm and 50 mm parallel plates with a gap of 1 mm. The procedure involved loading the sample, trimming the edge, and applying a thin layer of silicon oil to prevent moisture evaporation. The sample was then allowed to rest for 1 min before testing. Rheometer data were collected using the Anton Paar RheoCompass 1.22 system.

2.4.1. Rotation shear viscosity test

Rotation shear viscosity measurements were performed at shear rates ranging from 0.01 s^{-1} to 100 s^{-1}. Shear-thinning behavior was characterized using the power law model, and the consistency index (K) and flow index (n) were obtained from a linear regression of the linear region at logarithmic scales (Jagadiswaran et al., 2021):

$$\eta = K\,\dot{\gamma}^{(n-1)} \tag{1}$$

where η is viscosity (Pa·s), K is the consistency index (Pa.s^n) and $\dot{\gamma}$ is the shear rate (s^{-1}), and n is dimensionless. The coefficient of determination (R^2) was used to evaluate the fit.

2.4.2. Strain sweep test

Strain sweep tests were performed at a constant frequency of 6.28 rad/s, covering a strain range from 0.01% to 1000%, to determine the linear viscoelastic range (LVR). The yield stress was identified at the point of intersection between the storage modulus (G') and loss modulus (G") (Wilson et al., 2017).

2.4.3. Dynamic oscillation frequency sweep test

A dynamic oscillation frequency sweep was performed at a constant strain of 0.1% over a frequency range of 0.1 to 100 rad/s, within the LVR of the inks.

2.4.4. Three-interval thixotropy test

A three-interval thixotropy test was conducted to characterize the shear recoverability of inks by applying a low shear rate of 1 s^{-1} for 60 s, followed by a high shear rate of 100 s^{-1} for 60 s, and a low shear rate of 1 s^{-1} was applied for 60 s. The methodology was adopted from a previous study with minor modifications (Z. Liu et al., 2019), and the recovery rate was calculated based on a method described by (Toker et al., 2015).

2.5. 3D printing

The 3D models were designed using Autodesk Inventor Professional software (Autodesk 2023). Two different models were designed: for printability evaluation, a 3D hollow cube measuring 18.4 mm × 1.7 mm × 10 mm (Fig. S1A); and for texture property evaluation, a 3D parallelogram-shaped cuboid measuring 16 mm × 16 mm × 10 mm (Fig. S1B). To investigate the texture effect according to 3D-printer parameters, the nozzle diameter and infill density were chosen in the computer-aided design (CAD) model shown in Table S1. The models were then exported as.stl files and imported into Simplify 3D slicing software (ver.4.1.1). Printing was conducted using an extrusion-based 3D printer (LUCA, Illuminaid, South Korea.

2.6. Printability evaluation

To evaluate printability, the following settings were used: nozzle diameter = 0.85 mm, extrusion multiplier = 0.02 mm, and default speed = 420 mm/min (Fig. S1A). Printability was evaluated separately for height and width. The length of the width (top view) and height (front view) were measured from images using ImageJ, and average values were used for analysis. Percentage errors were then calculated for each dimension using Equation (2):

$$P_{error} = \frac{X_{measured} - Y_{designed}}{Y_{designed}} \times 100 \tag{2}$$

where P_{error} represents the percentage error, $X_{measured}$ is the average length (width or height), and $Y_{designed}$ is the corresponding designed length derived from the CAD design.

2.7. Textural analysis

To evaluate the textural similarity between the 3D-printed analogs

and actual fish (mackerel, salmon, and flounder), hardness and cohesiveness values were compared following a methodology developed by (Dunne et al., 2025; Souppez et al., 2025). Those studies conducted assessments based on whether the printed samples' values fell within the empirically defined reference ranges of steamed fish, rather than exact numerical correspondence. This range-based approach accounts for the natural variability of biological tissues.

All 3D-printed samples of WC 36% were fabricated as parallelogram-shaped cuboids (16 × mm × 16 mm × 10 mm) and subjected to texture profile analysis using a texture analyzer (TA. XT2i Plus, Stable Microsystem, Arrow Scientific Pty., Ltd). A 25 mm × 25 mm square probe was employed at a deformation rate of 30% and test speed of 1 mm/s. The measurement protocols were adapted from previously reported methodologies (Nam et al., 2023; Wen et al., 2022). For comparison, steamed-fish samples (mackerel, flounder, and salmon) with the same dimensions as the printed samples were prepared and tested under identical conditions following 4 min of steaming, followed by cooling at 25 °C for 15 min.

2.8. Statistical analysis

All results were presented as the mean ± standard deviation. All analyses were conducted in triplicate (n = 3). Statistical analysis was performed using one-way analysis of variance followed by Duncan's test using SPSS software (SPSS ver. 12.0, SPSS Inc., USA). A p value < 0.05 was considered statistically significant. Graphs were generated using SigmaPlot ver. 12.5 (Sigmasoft, USA).

3. Results and discussion

3.1. Determining the white chlorella concentration for optimal printing

3.1.1. Microstructure

The microstructures of WC ink with different concentrations (32%–40%) of microalga were visualized using an SEM (Fig. 1). A microstructural analysis revealed a porous network across all concentrations, which can contribute to the elasticity of the gels (Ran et al., 2022). The pore morphology appeared uniform, and the pores were predominantly elliptical (Fig. 1A–E). The average pore size decreased from 57.16 μm to 13.55 μm as the WC concentration increased from 32% to 40%, reflecting a denser network structure at a higher WC concentration (Du et al., 2013). Due to WC's hydrophilic compounds, its cell structure and high water-binding capacity contributed to the creation of a denser network at higher concentrations, which led to increased cross-linking (Uribe-Wandurraga et al., 2020). This suggests that increased cross-linking contributes to improved gel strength (Pant et al., 2021), which will be further corroborated by rheological analysis in the subsequent sections.

3.1.2. Extrusion-relevant flow behavior and power-law parameters

There are three major stages of printing; extrusion, printing, post-printing, and rheological properties provide direct information on ink behavior in each of these steps. For the first stage, extrusion, flow behavior of the ink is directly related to nozzle extrusion, because nozzle flow is governed by viscosity response under shear during printing (Amorim et al., 2021). In particular, a pseudoplastic property is critical for smooth extrusion through small nozzles, which in turn determines the quality of the printed objects (M. Wang et al., 2023). As shown in Fig. 2A, the viscosity of five inks decreased as the shear rate increased, confirming their non-Newtonian and pseudoplastic nature (Z. Liu et al., 2019). Flow index (n), a key parameter in the power-law model reflecting extrusion feasibility, was below 1 for all samples (Zhu et al., 2023), and decreased with increasing WC concentrations, indicating enhanced extrudability and more pronounced shear-thinning behavior (Fig. 2B). The power-law model adequately described the flow-curve data for all samples ($R^2 \geq 0.97$) (Table S2).

Another key parameter, the consistency index (K), increased nonlinearly and significantly from 133.78 Pa s to 2457.15 Pa s along with WC concentration. Taken together, the opposing trends of these two parameters indicate that WC inks at all concentrations exhibit shear-thinning behavior. This phenomenon may be attributable to interactions between algal cells and soluble polymers released into the medium, because microalgae cell aggregates are formed as biomass concentration increases (Souliès et al., 2013). The WC concentration increased only from 32% to 40% in 2% increments, while K increased nonlinearly by approximately 18-fold, suggesting a narrow process window in which improved shear-thinning may be accompanied by an elevated risk of nozzle-clogging at high K values (Z. Liu et al., 2019). Moreover, n and K primarily describe flow during extrusion and do not fully predict shape retention after deposition. Subsequent tests were therefore conducted to verify whether the extruded ink could maintain structural stability after printing.

3.1.3. Viscoelasticity governing yield behavior and post-deposition

Strain sweep tests were conducted to characterize the linear or nonlinear viscoelastic regions of structured fluid systems and to determine the yield stress (Fig. 3A). These moduli are crucial as they correlate closely with the stress required to initiate the flow (Corker et al., 2019). Sufficient yield stress is necessary to ensure that the printed material maintains its shape after exiting the nozzle and that the lower layers can support the weight of the layers above them (Chen et al., 2019). The yield stress at the intersection of G' and G" increased significantly at higher concentrations of WC ink, from 25.68 to 425.22 Pa (Table 1). A broader LVR was observed at lower biomass concentrations (WC 32% and WC 34%) compared with higher concentrations (WC 36%, WC 38%, and WC 40%) (Fig. 3A). These observations align with the findings of (Stickel et al., 2009), who reported that a higher biomass content increases particle interactions and structural complexity, leading to faster structural breakdown under stress and a narrower LVR. To ensure that all specimens were measured within the LVR range, a shear strain value of 0.1% was selected for the frequency sweep test across all samples (Fig. 3B). The results indicate that WC inks can flow while maintaining their structure under adequate stress, a characteristic particularly advantageous for 3D printing.

Frequency sweep tests were conducted to assess the viscoelastic properties of the inks. As illustrated in Fig. 3B, both G' and G" increased with angular frequency (from 0.1 rad/s to 100 rad/s), with G' consistently exceeding G". These results indicate that WC inks exhibit predominantly elastic behavior rather than viscous flow, suggesting a solid-like rheological profile advantageous for 3D printing of foods (Corker et al., 2019). This behavior is likely due to its composition of primarily proteins and polysaccharides (Jang et al., 2017). The interaction between these two components may enhance the structural properties of food gel, which is important to achieving the desirable rheological property (Banerjee & Bhattacharya, 2012). Moreover, a high G′ value signifies a strong anti-disintegration ability and hardness, and indicates that the material requires more energy to resist flow (Yunlei Fu et al., 2021). These trends support concentration-dependent differences in network strength, which can influence post-deposition shape retention during extrusion-based 3D printing.

3.1.4. Final formulation selection based on recovery behavior and dimensional fidelity

Three-interval thixotropic tests (3ITTs) were performed to approximate the low-high-low shear conditions during extrusion-based printing and to quantify viscosity breakdown and recovery as rheological indicators relevant to printing performance. (Chao et al., 2024). The viscosity profiles are presented in Fig. 4A. During the first low-shear interval (0–60 s), all formulations reached a steady viscosity plateau, with higher WC concentrations yielding higher viscosity levels. Upon shifting to the second interval (60–120 s) under high shear, a sharp decrease in viscosity was observed across all inks. The viscosities of WC

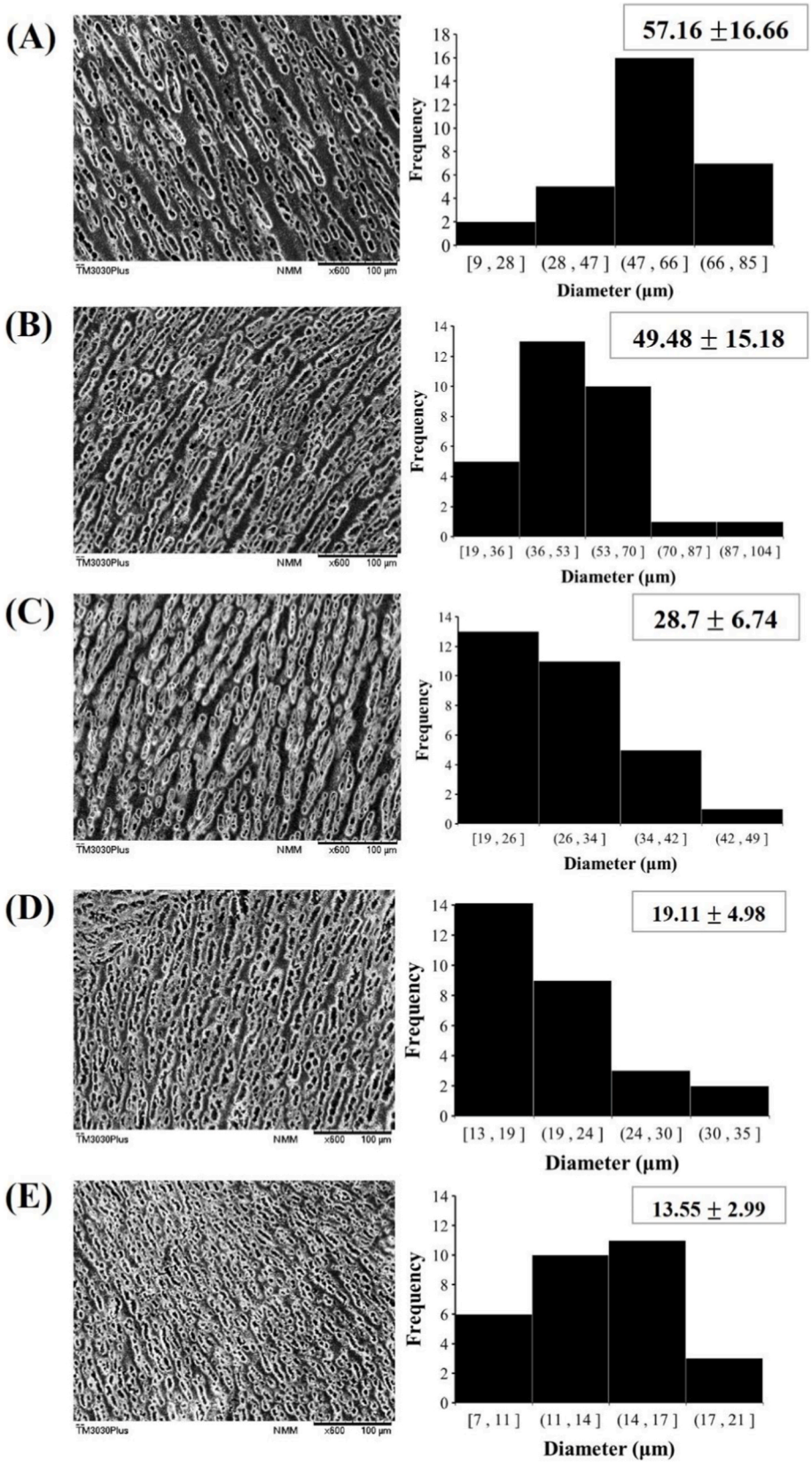


Fig. 1. SEM imaging and pore morphology characterization of white chlorella (WC) inks at different concentrations (left column) with the corresponding pore size distribution histograms (right column). (A) WC 32%, (B) WC 34%, (C) WC 36%, (D) WC 38%, and (E) WC 40%. Data are presented as mean ± SD (n = 3).

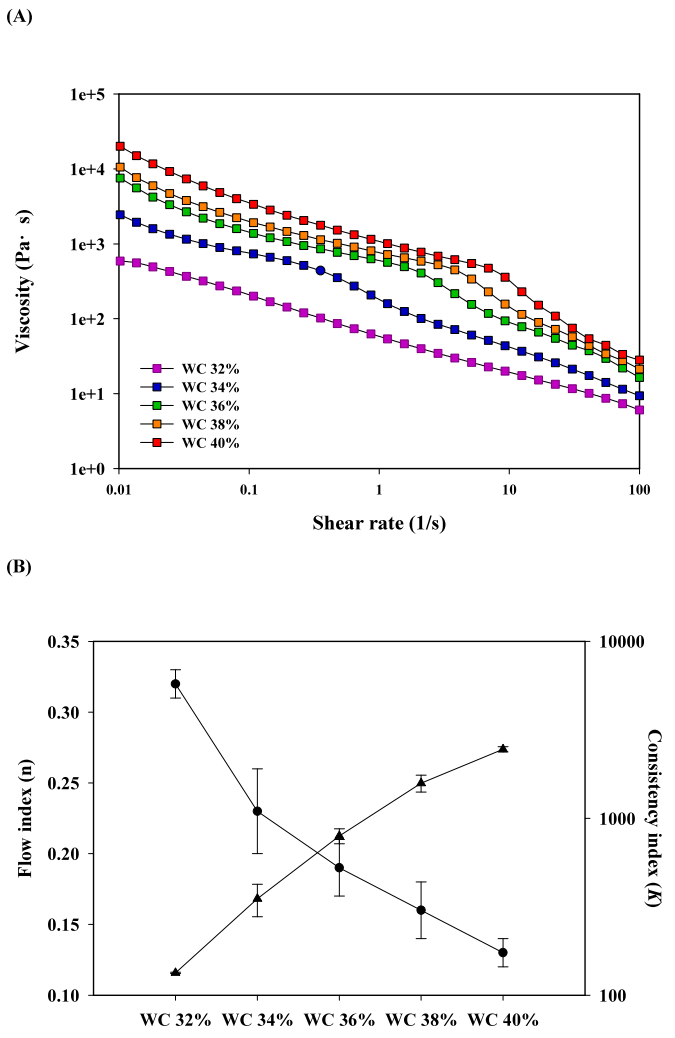


Fig. 2. Flow behavior characterization of white chlorella (WC) inks with varying concentrations. (A) Viscosity as a function of shear rate (0.01-100 s^{-1}), (B) Power-law model parameters obtained by fitting the flow curves; flow index (n) and consistency index (K). Data are presented as mean ± SD ($n = 3$).

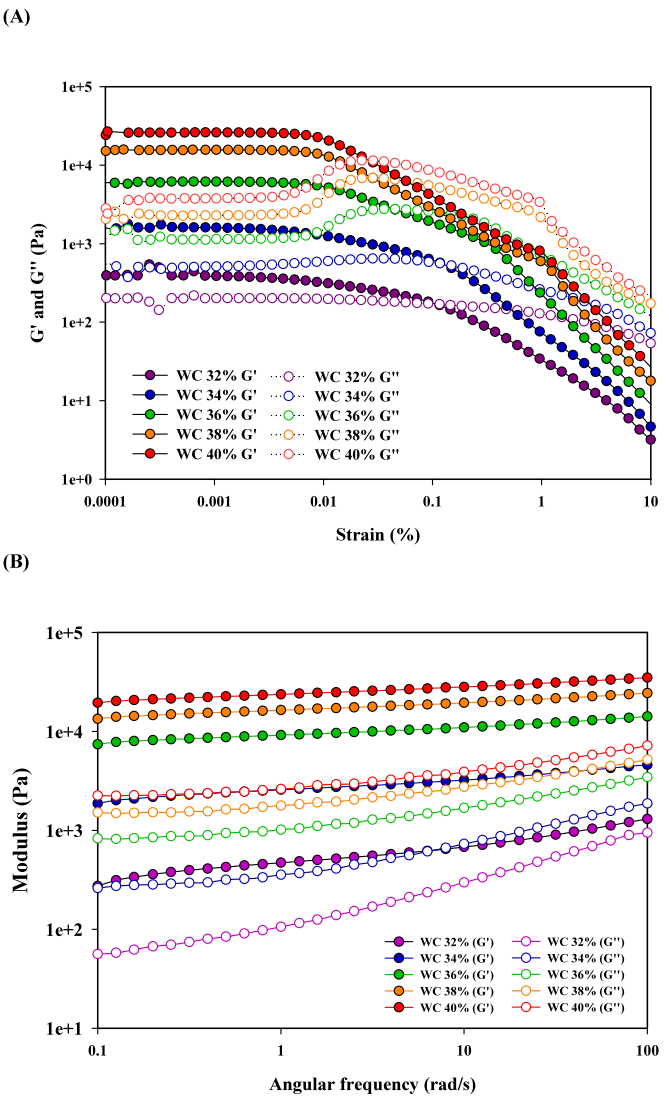


Fig. 3. Oscillatory viscoelastic properties of white chlorella (WC) inks. (A) Strain sweep tests showing the storage modulus(G') and loss modulus (G") as a function of strain amplitude at a fixed angular frequency of 6.28 rad/s. (B) Frequency sweep analysis showing storage modulus (G') and loss modulus (G") across angular frequencies (0.1-10 rad/s).

38% and WC 40% dropped below 1 Pa s, suggesting a significant breakdown of their internal structures. In contrast, WC 32%–36% maintained viscosities above 1 Pa s throughout this interval, with WC 36% exhibiting the most stable resistance to shear-induced thinning. Upon returning to low shear (120–180 s), WC 32%, WC 34%, and WC 36% recovered to 78%, 70%, and 60%, respectively (Fig. 4B), whereas WC 38% and WC 40% recovered by less than 5%, suggesting irreversible damage after strong deformation (Moakes et al., 2015). Importantly, 3ITTs quantify viscosity dynamics under controlled shear conditions, but these results alone cannot fully predict actual printing outcomes (Balters & Reichl, 2025).

Accordingly, printability was evaluated via the dimensional accuracy of the height and width of the printed objects. As shown in Fig. 5A–C, a hollow square printed with WC 36% remained structurally intact. WC 32% and, partly, WC 34% were extrudable but exhibited dimensional deviations. This is consistent with their lower G' compared with WC 36% (Fig. 3B), indicating insufficient elastic resistance for self-support. Higher concentrations have also been reported to reduce filament spreading during printing (Outrequin et al., 2024). Conversely, further increasing the WC concentration compromised extrusion. WC 38% exhibited under-extrusion, leading to deviations from the target width (−6%) and height (−61%), while WC 40% could not be extruded. This is consistent with its high apparent viscosity in the flow-curve tests (Fig. 2A) and predominantly solid-like viscoelastic response (Fig. 3B). Together, these results suggest an upper limit of the rheological printability window, beyond which continuous deposition of filaments is hindered and nozzle clogging is induced (Zhong et al., 2024).

Taken together, while 3ITTs effectively captured shear-induced breakdown and recovery, the resulting mismatch with dimensional accuracy indicated that the recovery ratio alone is insufficient and must be interpreted alongside buildability and extrudability metrics (Calafel et al., 2025). Consequently, WC 36% was identified as the practical optimum, providing sufficient post-deposition self-support without exceeding the extrusion limits of the printing system.

3.2. *Effect of printing parameters on 3D printed objects*

The impact of printing parameters on the samples was investigated while maintaining identical printing speed and pressure. Fig. 6 illustrates how variations in nozzle diameter and infill density affected the appearance and structure of WC 36% samples. The internal diameter of the nozzle correlates directly with the thickness of the extruded lines (Yang et al., 2018). The top-view images reveal that a smaller nozzle

Table 1
Measured yield stress of food inks with varying concentrations of white chlorella (WC).

Content	WC 32%	WC 34%	WC 36%	WC 38%	WC 40%
Yield stress τy (Pa)	25.68 ± 5.79^{e}	91.58 ± 20.70^{d}	171.84 ± 6.67^{c}	276.23 ± 10.98^{b}	425.22 ± 11.56^{a}

Equal letters in the same row indicate no statistically significant differences ($p < 0.05$).

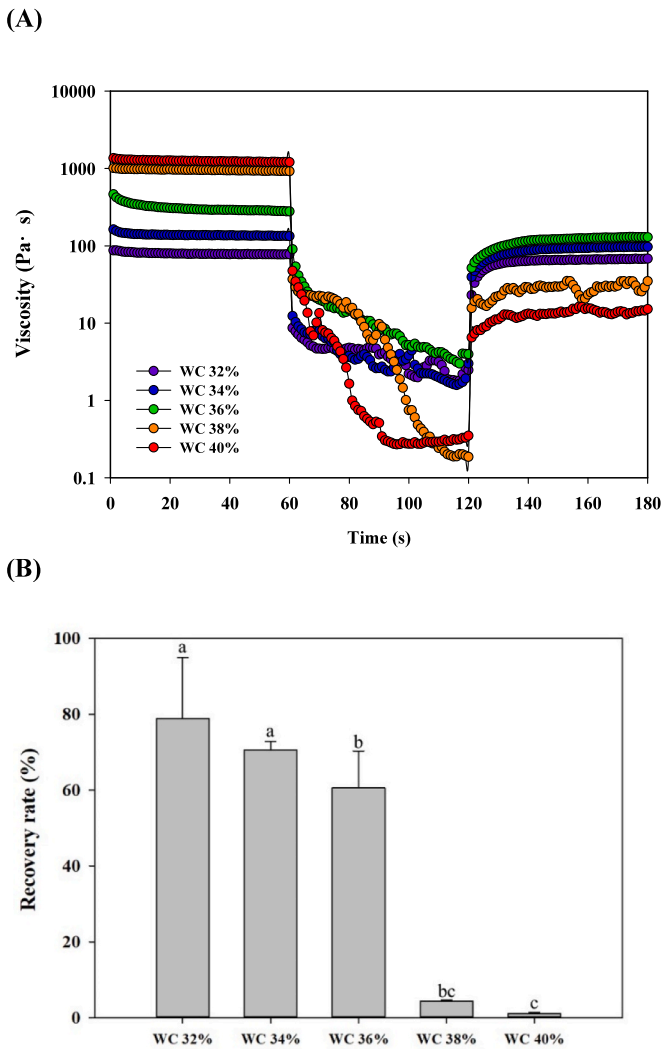


Fig. 4. Three-interval thixotropy and viscosity recovery of WC inks at different concentration. (A) Three-interval thixotropy test (3ITT) demonstrating viscosity recovery under shear rate changes. (B) Recovery rate calculated from (A). Different letters (a-c) indicate statistically significant differences ($p < 0.05$).

diameter produced more evenly extruded lines and surfaces (Thangalakshmi S, 2022), while larger nozzles led to less uniformity. This aligns with previous studies indicating that smaller nozzle sizes typically result in superior printing quality (Y. Liu, Liang, et al., 2019; Wang et al., 2018). Infill density, representing the proportion of the internal volume filled in a sample (Huang et al., 2019), also significantly affected the final structure. As the infill density increased, more internal pattern appeared to be more filled, with fewer visible gaps, which is consistent with increased ink extrusion. Overall, the deposited filaments followed the CAD-designed geometry across all conditions. However, larger nozzle diameters and higher infill densities tended to reduce feature fidelity at sharp corners, as evidenced by corner rounding in the top and panoramic views (Fig. 6), which is consistent with reports that printing resolution decreases as nozzle diameter increases.

3.3. Texture analysis of 3D-printed objects: hardness and cohesiveness for simulating a fish-like texture

3.3.1. Hardness and cohesiveness

Using a texture profile analysis (TPA), we evaluated whether 3D-printed WC 36% constructs can approximate the texture of steamed mackerel, salmon, and flounder. Hardness and cohesiveness were used as key metrices (Lee & Hashimoto, 2024) because hardness, defined as the force required to deform a material (Shaikh et al., 2017), affects mouthfeel and consumer perception (Bland et al., 2018; Zhang et al., 2021). Cohesiveness, representing the interparticle bonding strength that allows a product to resist compaction without disintegrating during chewing, is another critical attribute (Dong, 2023). The measured hardness and cohesiveness values of fish samples (Fig. 7B and D) are presented alongside those of the printed sample data (Fig. 7A and C).

As infill density increased, hardness increased at all nozzle diameters (Fig. 7A). The effect was strongest for the 0.5 mm nozzle, showing an increase of approximately 18%, from 30% to 60% infill, and a further increase of approximately 40%, from 60% to 90%. In contrast, 0.85 mm and 1.2 mm nozzles exhibited smaller increases (~6% and ~10% from 30% to 60%), with only limited additional gains at 90% of infill density. This observations are consistent with reports that increasing infill promotes material deposition and consolidation, thereby increasing hardness (Carranza et al., 2023). Notably, the increment of hardness plateaued at a higher infill for the larger nozzles, suggesting diminishing nozzle-dependent returns (Maguluri et al., 2022). This may be because larger nozzle diameters increase inter-filament void between adjacent filaments, which limits effective densification (Fig. 6). Consequently, hardness becomes less sensitive to further increases in infill at higher values (Czyżewski et al., 2022).

Cohesiveness exhibited a parallel trend with the hardness values, with the 0.5 mm nozzle achieving a consistent increase in cohesiveness, from 30% to 90% infill density (Fig. 7C), likely resulting from progressively tighter interparticle bonding as the density increased (Huang et al., 2019; Thangalakshmi S, 2022). In contrast, the 0.85 mm and 1.2 mm nozzles displayed a cohesion pattern similar to that of hardness, showing an increase of up to 60% infill density before plateauing. To be more specific, the 0.85 mm nozzle followed a similar but less-gradual trend, while the 1.2 mm nozzle, with its reduced ability to fill finer gaps, showed no increase in cohesiveness beyond an infill density of 60%. This observation differs from findings by (Yu et al., 2023), who reported that higher infill densities typically reduce internal voids and enhance structural compactness. In the current study, however, the internal structure appeared to achieve maximal effective contact between particles at approximately 60% infill density, beyond which additional material did not enhance cohesiveness significantly (Yuan et al., 2022). This indicates that larger nozzle diameters may facilitate the early onset of structural saturation, where interparticle bonding reaches an optimal threshold within the tested parameter range (D. Wang, Lu, et al., 2023). For larger nozzles, increasing the infill beyond 60% offered limited gains in hardness and cohesiveness. As a result, nozzle-infill selection should be guided by the targeted texture.

While trends in hardness and cohesiveness were identified across varying printing parameters, a quantitative analysis of correlations between specific printing parameters and these textural properties was not undertaken in this study. Future research should investigate these relationships in greater depth to optimize the texture of 3D-printed materials.

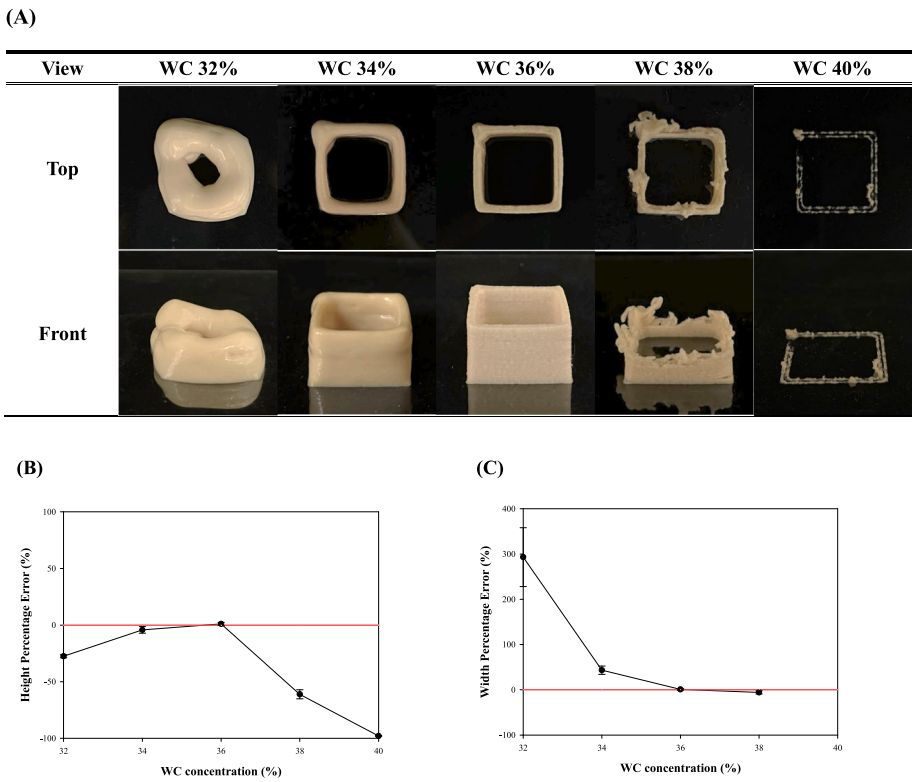


Fig. 5. Printability evaluation of 3D-printed white chlorella (WC) inks at different concentrations. (A) Representative hollow square prints (top and front views). (B) Height error relative to the target dimension (%), (C) Width error relative to the target dimension (%).

3.3.2. *Simulating fish-like texture*

Because fish hardness is species-dependent due to differences in muscle structure and composition, the hardness values of steamed mackerel (575.21 g), flounder (659.77 g), and salmon (788.36 g) were used as species-specific targets (Fig. 7B and D) (Wu et al., 2014). Within the tested nozzle-infill parameter ranges, these targets were reached by co-adjusting the nozzle diameter and infill density (Fig. 7A and C). Specifically, mackerel hardness was obtained at a range of either 0.85 mm and 30% or 0.5 mm and 60%, flounder at either 0.5 mm and 30% or 0.85 mm and 60%, and salmon at either 1.2 mm 60% or 0.5 mm and 90%. These data indicate that comparable target hardness values can be achieved by multiple nozzle-infill combinations. Such parameters provide design flexibility whereby parameter selection can be guided by practical printing performance while maintaining the primary texture targets (Pereira et al., 2021). These findings emphasize that specific nozzle and density settings can closely approximate the hardness of different species through 3D-printed WC ink (Z. Liu & Zhang, 2021).

Cohesiveness was more difficult to match across species, indicating that it acts as a limiting metric within parameter combinations in this system. As shown in Fig. 7B and D, cohesiveness differed across fish species, due to intrinsic mechanical properties, such as muscle fiber structure and fat content, which influenced both texture and firmness (Bugeon et al., 2003). As shown in Fig. 7B, the cohesiveness of mackerel (0.73) was effectively reproduced within the texture range of the WC samples. The use of an infill density of 60% and a nozzle diameter of 0.85 mm enabled the replication of mackerel's cohesiveness, demonstrating the potential of adjusting the 3D-printing parameters to emulate specific fish textures (Schreuders et al., 2021; Xu et al., 2016). In contrast, achieving comparable cohesiveness values for salmon (0.42) and flounder (0.78) was challenging. The firmer texture of flounder is possibly related to its high protein content, while the reduced cohesiveness of salmon may be attributable to its higher fat levels (Fomena Temgoua et al., 2022; Kim et al., 2012). These findings emphasize the need to apply adequate printing parameters to 3D-printed samples to replicate the textural properties of salmon, mackerel, and flounder within targeted texture ranges.

4. Conclusion

This study developed an *A. protothecoides* food ink for extrusion-based 3D printing to emulate fish-like texture. Overall, increasing the WC concentration led to a denser microstructural network and enhanced yield behavior, and storage moduli consistently exceeded loss moduli. Notably, thixotropic recovery rates were not predictive as assessed by dimensional fidelity. Lower concentrations (WC 32%, 34%) led to filament spreading, while higher concentrations resulted in under-extrusion (WC 38%) or extrusion failure (WC 40%). Consequently, a narrow printable window was identified at WC 36%, which yielded the most stable constructs despite showing no peak recovery rate. Subsequently, a TPA was conducted on WC 36% products to evaluate the effect of nozzle diameter and infill density. For larger nozzles (0.85 and 1.2 mm in diameter), increasing the infill density beyond 60% offered limited gains in hardness and cohesiveness. Finally, when compared to steamed fish, while multiple nozzle-infill combinations could match the target hardness, cohesiveness was specifically matched only for mackerel.

These findings establish a formulation-rheology-printing framework for developing microalga-based ink with tunable textural profiles. By using a minimalistic ingredient approach, WC-based inks offer a promising clean-label platform for fabricating structured seafood analogs while minimizing formulation complexity and reliance on exogenous structuring agents. Although this study focused on feasibility, future research incorporating broader parameter mapping (e.g., design of experiments) may further refine the design of sophisticated fish-like analogs.

CRediT authorship contribution statement

Yurim Ha: Writing – original draft, Visualization, Methodology,

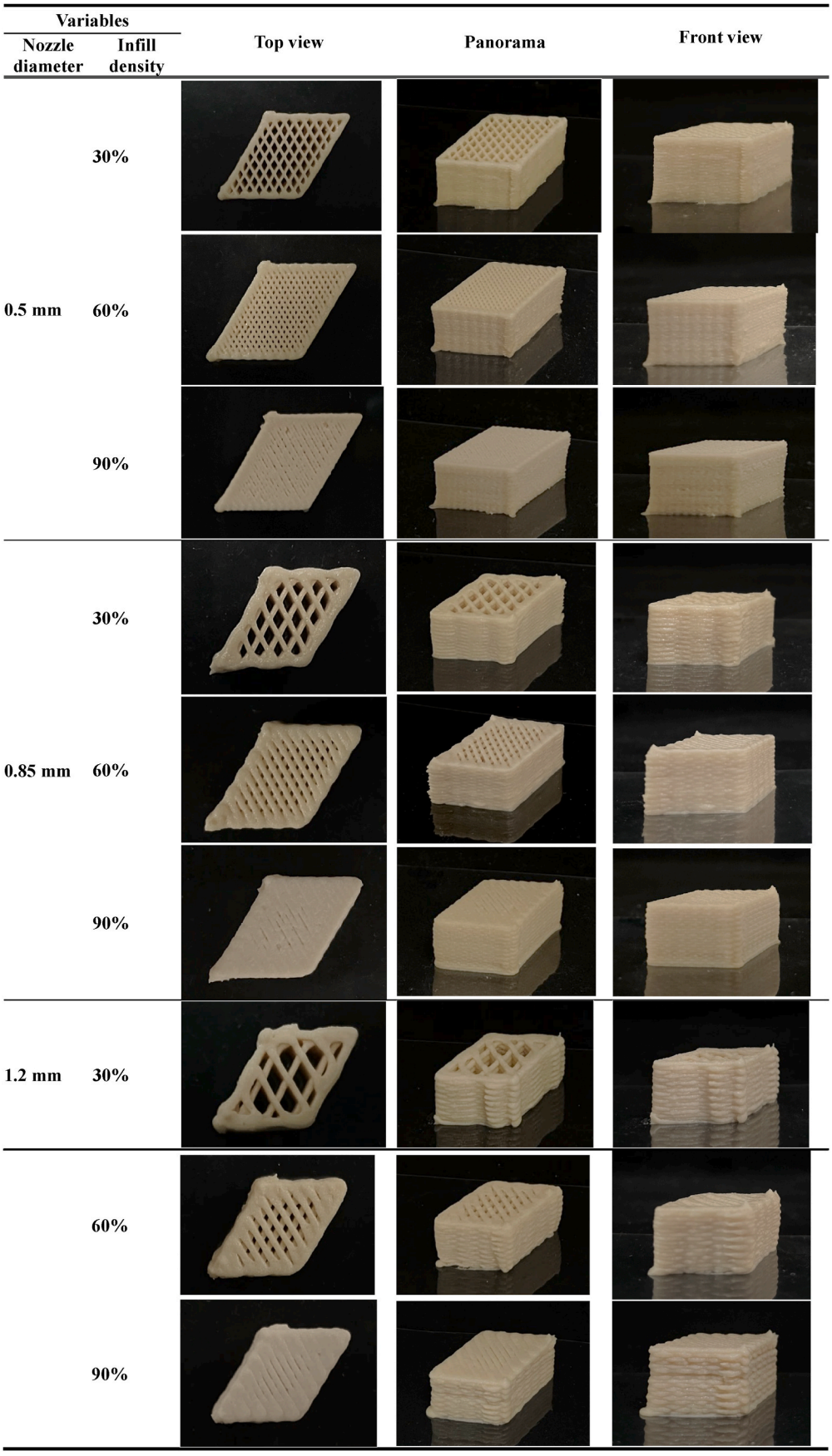


Fig. 6. Representative images of 3D printed objects with different infill densities (30%, 60% and 90%) and filament diameters (0.5 mm, 0.85 mm and 1.2 mm).

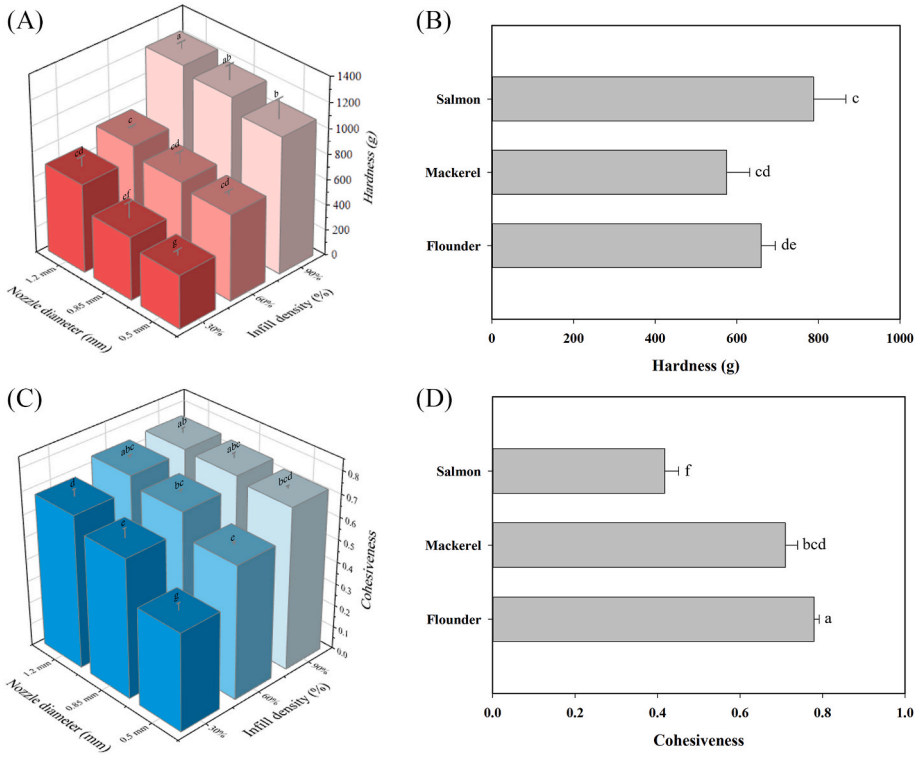


Fig. 7. Textural properties of 3D-printed WC samples and steam-cooked fish species (mackerel, flounder, and salmon). (A) Hardness values of printed samples under varying infill densities and nozzle diameters. (B) Reference hardness values of steam fish samples (mackerel, flounder, and salmon), serving as target benchmarks for assessing the textural fidelity of the 3D-printed samples. (C) Cohesiveness values of WC-printed samples under the same printing conditions. (D) Reference cohesiveness values of steam fish samples (mackerel, flounder, and salmon), serving as target benchmarks for assessing the textural fidelity of the 3D-printed samples. All analyses were conducted in triplicate (n = 3). Different superscript letters indicate significant differences ($p < 0.05$) according to Duncan's multiple range test.

Investigation, Formal analysis, Data curation, Conceptualization. **Eui-Jung Han:** Writing – review & editing, Visualization, Methodology, Investigation, Formal analysis, Data curation, Conceptualization. **Yourim Oh:** Writing – review & editing, Methodology, Conceptualization. **Jin-Kyu Rhee:** Supervision, Project administration, Funding acquisition.

Declaration of generative AI and AI-assisted technologies in the writing process

During the preparation of this work the authors used Chat GPT and Gemini to improve the readability and language of the manuscript. After using this tool/service, the authors reviewed and edited the content as needed and we take full responsibility for the content of the published article.

Declaration of competing interest

The authors have no conflicts of interest to declare.

Acknowledgments

This research was supported by the Korea Institute of Marine Science & Technology Promotion funded by the Ministry of Oceans and Fisheries (RS-2024-00402200); and by the National Research Foundation of Korea grant funded by the Korea government (No. RS-2025-00519539); and by the Korea Institute of Planning and Evaluation for Technology in Food, Agriculture and Forestry through the High Value-added Food Technology Development Program, funded by the Ministry of Agriculture, Food and Rural Affairs (RS-2024-00404751). This work was also supported by the Technology Development Program (RS-2024-00468447), funded by the Ministry of SMEs and Startups.

Appendix A. Supplementary data

Supplementary data to this article can be found online at https://doi.org/10.1016/j.lwt.2026.119277.

Data availability

Data will be made available on request.

References

Amorim, P., d'Ávila, M., Anand, R., Moldenaers, P., Van Puyvelde, P., & Bloemen, V. (2021). Insights on shear rheology of inks for extrusion-based 3D bioprinting. *Bioprinting, 22*, Article e00129.

Balters, L., & Reichl, S. (2025). A design of experiment to evaluate the printability for bioprinting by using deep learning image similarity. *Journal of Biomedical Materials Research Part A, 113*(7), Article e37961.

Banerjee, S., & Bhattacharya, S. (2012). Food gels: Gelling process and new applications. *Critical Reviews in Food Science and Nutrition, 52*(4), 334–346. https://doi.org/10.1080/10408398.2010.500234. PMID: 22332597.

Batista, A. P., Niccolai, A., Fradinho, P., Fragoso, S., Bursic, I., Rodolfi, L., Biondi, N., Tredici, M. R., Sousa, I., & Raymundo, A. (2017). Microalgae biomass as an alternative ingredient in cookies: Sensory, physical and chemical properties, antioxidant activity and in vitro digestibility. *Algal Research, 26*, 161–171. https://doi.org/10.1016/j.algal.2017.07.017

Bland, J. M., Bett-Garber, K. L., Li, C. H., Brashear, S. S., Lea, J. M., & Bechtel, P. J. (2018). Comparison of sensory and instrumental methods for the analysis of texture of cooked individually quick frozen and fresh-frozen catfish fillets. *Food Science and Nutrition, 6*(6), 1692–1705. https://doi.org/10.1002/fsn3.737

Bugeon, J., Lefevre, F., & Fauconneau, B. (2003). Fillet texture and muscle structure in brown trout (Salmo trutta) subjected to long-term exercise. *Aquaculture Research, 34*(14), 1287–1295. https://doi.org/10.1046/j.1365-2109.2003.00938.x

Calafel, M. I., Criado-Gonzalez, M., Aguirresarobe, R., Fernández, M., & Mijangos, C. (2025). From rheological concepts to additive manufacturing assessment of

hydrogel-based materials for advanced bioprinting applications. *Materials Advances, 6*(14), 4566–4597.
Canelli, G., Tarnutzer, C., Carpine, R., Neutsch, L., Bolten, C. J., Dionisi, F., & Mathys, A. (2020). Biochemical and nutritional evaluation of Chlorella and Auxenochlorella biomasses relevant for food application. *Frontiers in Nutrition, 7*, Article 565996.
Carranza, T., Guerrero, P., de la Caba, K., & Etxabide, A. (2023). Texture-modified soy protein foods: 3D printing design and red cabbage effect. *Food Hydrocolloids, 145*, Article 109141.
Chao, E., Yan, X., & Fan, L. (2024). Fabrication of edible inks for 3D printing as a dysphagia food: An emerging application of bigels. *Food Hydrocolloids*. , Article 110463. https://doi.org/10.1016/j.foodhyd.2024.110463
Chen, H., Xie, F., Chen, L., & Zheng, B. (2019). Effect of rheological properties of potato, rice and corn starches on their hot-extrusion 3D printing behaviors. *Journal of Food Engineering, 244*, 150–158. https://doi.org/10.1016/j.jfoodeng.2018.09.011
Chen, Y., Zhang, M., Sun, Y., & Phuhongsung, P. (2022). Improving 3D/4D printing characteristics of natural food gels by novel additives: A review. *Food Hydrocolloids, 123*, Article 107160. https://doi.org/10.1016/j.foodhyd.2021.107160
Clydesdale, F. M. (1993). Color as a factor in food choice. *Critical Reviews in Food Science and Nutrition, 33*(1), 83–101. https://doi.org/10.1080/10408399309527614
Coleman, B., Van Poucke, C., Dewitte, B., Ruttens, A., Moerdijk-Poortvliet, T., Latsos, C., De Reu, K., Blommaert, L., Duquenne, B., Timmermans, K., van Houcke, J., Muylaert, K., & Robbens, J. (2022). Potential of microalgae as flavoring agents for plant-based seafood alternatives. *Future Foods, 5*, Article 100139.
Corker, A., Ng, H. C. H., Poole, R. J., & García-Tuñón, E. (2019). 3D printing with 2D colloids: Designing rheology protocols to predict "printability' of soft-materials. *Soft Matter, 15*(6), 1444–1456. https://doi.org/10.1039/C8SM01936C
Czyżewski, P., Marciniak, D., Nowinka, B., Borowiak, M., & Bieliński, M. (2022). Influence of extruder's nozzle diameter on the improvement of functional properties of 3D-printed PLA products. *Polymers, 14*(2), 356.
Dong, X. (2023). Texture of fish and fish products. *Food Texturology: Measurement and Perception of Food Textural Properties*, 331–353. https://doi.org/10.1007/978-3-031-41900-3_16
Du, L., Khiari, Z., Pietrasik, Z., & Betti, M. (2013). Physicochemical and functional properties of gelatins extracted from Turkey and chicken heads. *Poultry Science, 92*(9), 2463–2474. https://doi.org/10.3382/ps.2013-03161
Dunne, R. A., Darwin, E. C., Medina, V. A. P., Levenston, M. E., Pierre, S. R. S., & Kuhl, E. (2025). Texture profile analysis and rheology of plant-based and animal meat. *Food Research International*. , Article 115876. https://doi.org/10.1016/j.foodres.2025.115876
FAO. (2024). *FAO report: Global fisheries and aquaculture production reaches a new record high*. Newsroom.
Fomena Temgoua, N. S., Sun, Z., Okoye, C. O., & Pan, H. (2022). Fatty acid profile, physicochemical composition, and sensory properties of Atlantic salmon fish (Salmo salar) during different culinary treatments. *Journal of Food Quality, 2022*(1), Article 7425142. https://doi.org/10.1155/2022/7425142
García-Segovia, P., Pagán-Moreno, M. J., Lara, I. F., & Martínez-Monzó, J. (2017). Effect of microalgae incorporation on physicochemical and textural properties in wheat bread formulation. *Food Science and Technology International, 23*(5), 437–447. https://doi.org/10.1177/1082013217700259
Huang, M.-s., Zhang, M., & Bhandari, B. (2019). Assessing the 3D printing precision and texture properties of brown rice induced by infill levels and printing variables. *Food and Bioprocess Technology, 12*, 1185–1196. https://doi.org/10.1007/s11947-019-02287-x
Jagadiswaran, B., Alagarasan, V., Palanivelu, P., Theagarajan, R., Moses, J., & Anandharamakrishnan, C. (2021). Valorization of food industry waste and by-products using 3D printing: A study on the development of value-added functional cookies. *Future Foods, 4*, Article 100036. https://doi.org/10.1016/j.fufo.2021.100036
Jang, H. S., Kang, N. S., Kim, K. M., Jeon, B. H., Park, J. S., & Hong, J. W. (2017). Description and application of a marine microalga Auxenochlorella protothecoides isolated from Ulleung-do. *Journal of Life Science, 27*(10), 1152–1160. https://doi.org/10.5352/JLS.2017.27.10.1152
Kim, D.-K., Kim, K.-D., Seo, J.-Y., & Lee, S.-M. (2012). Effects of dietary lipid source and level on growth performance, blood parameters and flesh quality of sub-adult olive flounder (Paralichthys olivaceus). *Asian-Australasian Journal of Animal Sciences, 25*(6), 869. https://doi.org/10.5713/ajas.2011.11470
Lee, C. P., & Hashimoto, M. (2024). Prediction of textural properties of 3D-printed food using response surface methodology. *Heliyon, 10*(7), Article e27658. https://doi.org/10.1016/j.heliyon.2024.e27658
Li, Y., Xiang, N., Zhu, Y. Y., Yang, M., Shi, C. C., Tang, Y. A., Sun, W. J., Sheng, K. C., Liu, D. H., & Zhang, X. M. (2024). Blue source-based food alternative proteins: Exploring aquatic plant-based and cell-based sources for sustainable nutrition. *Trends in Food Science & Technology, 147*, Article 104439. https://doi.org/10.1016/j.tifs.2024.104439
Liu, Z., Bhandari, B., Prakash, S., Mantihal, S., & Zhang, M. (2019). Linking rheology and printability of a multicomponent gel system of carrageenan-xanthan-starch in extrusion based additive manufacturing. *Food Hydrocolloids, 87*, 413–424. https://doi.org/10.1016/j.foodhyd.2018.08.026
Liu, Y., Liang, X., Saeed, A., Lan, W., & Qin, W. (2019). Properties of 3D printed dough and optimization of printing parameters. *Innovative Food Science & Emerging Technologies, 54*, 9–18. https://doi.org/10.1016/j.ifset.2019.03.008
Liu, Z., & Zhang, M. (2021). Texture properties of microwave post-processed 3D printed potato snack with different ingredients and infill structure. *Future Foods, 3*, Article 100017. https://doi.org/10.1016/j.fufo.2021.100017
Liu, Z., Zhang, M., & Yang, C.-h. (2018). Dual extrusion 3D printing of mashed potatoes/strawberry juice gel. *LWT, 96*, 589–596. https://doi.org/10.1016/j.lwt.2018.06.014
Maguluri, N., Suresh, G., & Guntur, S. R. (2022). Effect of printing parameters on the hardness of 3D printed poly-lactic acid parts using DOE approach. *IOP Conference Series: Materials Science and Engineering*.
Maldonado-Rosas, R., Tejada-Ortigoza, V., Cuan-Urquizo, E., Mendoza-Cachu, D., Morales-de La Pena, M., Alvarado-Orozco, J. M., & Campanella, O. H. (2022). Evaluation of rheology and printability of 3D printing nutritious food with complex formulations. *Additive Manufacturing, 58*, Article 103030.
Mantihal, S., Kobun, R., & Lee, B.-B. (2020). 3D food printing of as the new way of preparing food: A review. *International Journal of Gastronomy and Food Science, 22*, Article 100260. https://doi.org/10.1016/j.ijgfs.2020.100260
Mirzapour-Kouhdasht, A., Biparva, P., McClements, D. J., Garavand, F., & Garcia-Vaquero, M. (2024). Formulation of inks for 3D printing of microalgae-based meat analogues and the role of modified starch: A review. *International Journal of Food Science and Technology*. https://doi.org/10.1111/ijfs.17080
Moakes, R., Sullo, A., & Norton, I. (2015). Preparation and characterisation of whey protein fluid gels: The effects of shear and thermal history. *Food Hydrocolloids, 45*, 227–235.
Nam, H. K., Kang, T. W., Kim, I.-W., Choi, R.-Y., Kim, H. W., & Park, H. J. (2023). Physicochemical properties of cricket (Gryllus bimaculatus) gel fraction with soy protein isolate for 3D printing-based meat analogue. *Food Bioscience, 53*, Article 102772. https://doi.org/10.1016/j.fbio.2023.10277
Oh, Y., Lee, S., Lee, N. K., & Rhee, J. K. (2024). Improving the three-dimensional printability of potato starch loaded onto food ink. *Journal of Microbiology and Biotechnology, 34*(4), 891–901. https://doi.org/10.4014/jmb.2311.11040
Outrequin, T. C. R., Gamonpilas, C., Sreearunothai, P., Deepaisarn, S., & Siriwatwechakul, W. (2024). Machine learning assisted evaluation of the filament spreading during extrusion-based 3D food printing: Impact of the rheological and printing parameters. *Journal of Food Engineering, 381*, Article 112166.
Pant, A., Lee, A. Y., Karyappa, R., Lee, C. P., An, J., Hashimoto, M., Tan, U. X., Wong, G., Chua, C. K., & Zhang, Y. (2021). 3D food printing of fresh vegetables using food hydrocolloids for dysphagic patients. *Food Hydrocolloids, 114*, Article 106546. https://doi.org/10.1016/j.foodhyd.2020.106546
Pereira, T., Barroso, S., & Gil, M. M. (2021). Food texture design by 3D printing: A review. *Foods, 10*(2), 320.
Ran, X., Lou, X., Zheng, H., Gu, Q., & Yang, H. (2022). Improving the texture and rheological qualities of a plant-based fishball analogue by using konjac glucomannan to enhance crosslinks with soy protein. *Innovative Food Science & Emerging Technologies, 75*, Article 102910. https://doi.org/10.1016/j.ifset.2021.102910
Schreuders, F. K. G., Schlangen, M., Kyriakopoulou, K., Boom, R. M., & van der Goot, A. J. (2021). Texture methods for evaluating meat and meat analogue structures: A review. *Food Control, 127*, Article 108103. https://doi.org/10.1016/j.foodcont.2021.108103
Shaikh, M., Ali, T. M., & Hasnain, A. (2017). Utilization of chemically modified pearl millet starches in preparation of custards with improved cold storage stability. *International Journal of Biological Macromolecules, 104*, 360–366. https://doi.org/10.1016/j.ijbiomac.2017.05.183
Shi, H., Li, J., Xu, E., Yang, H., Liu, D., & Yin, J. (2023). Microscale 3D printing of fish analogues using soy protein food ink. *Journal of Food Engineering, 347*, Article 111436. https://doi.org/10.1016/j.jfoodeng.2023.111436
Souliès, A., Pruvost, J., Legrand, J., Castelain, C., & Burghelea, T. I. (2013). Rheological properties of suspensions of the green microalga Chlorella vulgaris at various volume fractions. *Rheologica Acta, 52*(6), 589–605. https://doi.org/10.1007/s00397-013-0700-z
Souppez, J.-B. R., Dages, B. A., Pavar, G. S., Fabian, J., Thomas, J. M., & Theodosiou, E. (2025). Mechanical properties and texture profile analysis of beef burgers and plant-based analogues. *Journal of Food Engineering, 385*, Article 112259. https://doi.org/10.1016/j.jfoodeng.2024.112259
Stickel, J. J., Knutsen, J. S., Liberatore, M. W., Luu, W., Bousfield, D. W., Klingenberg, D. J., Scott, C. T., Root, T. W., Ehrhardt, M. R., & Monz, T. O. (2009). Rheology measurements of a biomass slurry: An inter-laboratory study. *Rheologica Acta, 48*, 1005–1015. https://doi.org/10.1007/s00397-009-0382-8
Teixeira, C. M., & Silva, P. M. (2024). The huge dilemma: How to increase seafood consumption for health benefits without impacting fisheries' sustainability? *International Journal of Food Science and Technology, 59*(2), 661–672. https://doi.org/10.1111/ijfs.16841
Thangalakshmi S, V. K. A. V. P. (2022). Printability assessment and optimization of process parameters for 3D printing of rice flour and jaggery paste. *Journal of Biosystems Engineering, 47*(2), 248–262. https://doi.org/10.1007/s42853-022-00143-z
Toker, O. S., Karasu, S., Yilmaz, M. T., & Karaman, S. (2015). Three interval thixotropy test (3ITT) in food applications: A novel technique to determine structural regeneration of mayonnaise under different shear conditions. *Food Research International, 70*, 125–133.
Torres-Tiji, Y., Fields, F. J., & Mayfield, S. P. (2020). Microalgae as a future food source. *Biotechnology Advances, 41*, Article 107536. https://doi.org/10.1016/j.biotechadv.2020.107536
Uribe-Wandurraga, Z. N., Zhang, L., Noort, M. W. J., et al. (2020). Printability and physicochemical properties of microalgae-enriched 3D-Printed snacks. *Food and Bioprocess Technology, 13*(11), 2029–2042. https://doi.org/10.1007/s11947-020-02544-4
Wang, D., Guo, J., Wang, Y., Yang, Y., Jiang, B., Li, D., Feng, Z., & Liu, C. (2023). Whey protein isolate nanofibrils as emulsifying agent to improve printability of Cheddar cheese for 3D printing. *Food Hydrocolloids, 142*, Article 108807. https://doi.org/10.1016/j.foodhyd.2023.108807
Wang, M., Lu, X., Zheng, X., Li, W., Wang, L., Qian, Y., & Zeng, M. (2023). Rheological and physicochemical properties of Spirulina platensis residues-based inks for

extrusion 3D food printing. *Food Research International, 169*, Article 112823. https://doi.org/10.1016/j.foodres.2023.112823

Wang, L., Zhang, M., Bhandari, B., & Yang, C. (2018). Investigation on fish surimi gel as promising food material for 3D printing. *Journal of Food Engineering, 220*, 101–108. https://doi.org/10.1016/j.jfoodeng.2017.02.029

Wen, Y., Kim, H. W., & Park, H. J. (2022). Effect of xylose on rheological, printing, color, texture, and microstructure characteristics of 3D-printable colorant-containing meat analogs based on mung bean protein. *Food Research International, 160*, Article 111704. https://doi.org/10.1016/j.foodres.2022.111704

Wilson, S. A., Cross, L. M., Peak, C. W., & Gaharwar, A. K. (2017). Shear-thinning and thermo-reversible nanoengineered inks for 3D bioprinting. *ACS Applied Materials & Interfaces, 9*(50), 43449–43458.

Wu, D., Sun, D.-W., & He, Y. (2014). Novel non-invasive distribution measurement of texture profile analysis (TPA) in salmon fillet by using visible and near infrared hyperspectral imaging. *Food Chemistry, 145*, 417–426.

Xu, Y. S., Chen, Y. P., Cao, Y. Q., Huang, W. X., Zhang, S. C., Xia, W. S., & Jiang, Q. X. (2016). Effect of steam cooking on textural properties and taste compounds of shrimp (Metapenaeus ensis). *Food Science and Technology Research, 22*(1), 75–81. https://doi.org/10.3136/fstr.22.75

Yang, F. L., Zhang, M., Bhandari, B., & Liu, Y. P. (2018). Investigation on lemon juice gel as food material for 3D printing and optimization of printing parameters. *LWT, 87*, 67–76. https://doi.org/10.1016/j.lwt.2017.08.054

Yu, X., Wang, Y., Zhao, W., Li, S., Pan, J., Prakash, S., & Dong, X. (2023). Hydrophilic colloids (Konjac gum/Xanthan gum) in 3D printing of transitional food from fish paste. *Food Hydrocolloids, 137*, Article 108333. https://doi.org/10.1016/j.foodhyd.2022.108333

Yuan, Q., Xie, Z., Yao, H., Huang, T., Li, Z., & Zheng, X. (2022). Effect of polyacrylamide on the workability and interlayer interface properties of 3D printed cementitious materials. *Journal of Materials Research and Technology, 19*, 3394–3405. https://doi.org/10.1016/j.jmrt.2022.06.093

Yunlei Fu, T. C., Chen, S. H. Y., Liu, B., Sun, P., Han, S., & Chen, F. (2021). The potentials and challenges of using microalgae as an ingredient to produce meat analogues. *Trends in Food Science & Technology, 112*, 188–200. https://doi.org/10.1016/j.tifs.2021.03.050

Zhang, Z. Y., Pham, H., Tan, Y. B., Zhou, H. L., & McClements, D. J. (2021). Investigation of protein denaturation and textural changes of Atlantic salmon during simulated cooking. *Food Biophysics, 16*(4), 512–519. https://doi.org/10.1007/s11483-021-09690-y

Zhong, Q., Chen, Y., Zhang, X., Yang, G., Jin, W., Peng, D., & Huang, Q. (2024). Correlation between 3D printability and rheological properties of biopolymer fluid: A case study of alginate-based hydrogels. *Journal of Food Engineering, 370*, Article 111970.

Zhong, C., Feng, Y., & Xu, Y. (2023). Production of fish analogues from plant proteins: Potential strategies, challenges, and outlook. *Foods, 12*(3), 614. https://doi.org/10.3390/foods12030614

Zhu, J. C., Cheng, Y., Ouyang, Z. Y., Yang, Y. X., Ma, L., Wang, H. X., & Zhang, Y. H. (2023). 3D printing surimi enhanced by surface crosslinking based on dry-spraying transglutaminase, and its application in dysphagia diets. *Food Hydrocolloids, 140*, Article 108600. https://doi.org/10.1016/j.foodhyd.2023.108600